Fusion reactions in collisions of neutron halo nuclei with heavy targets

J. L. Ferreira,[1,*] J. Rangel,[2,1,†] J. Lubian,[1,‡] and L. F. Canto[3,§]

[1]*Instituto de Física, Universidade Federal Fluminense, Av. Litoranea s/n, Gragoatá, Niterói, Rio de Janeiro 24210-340, Brazil*

[2]*Departamento de Matemática, Física e Computação Universidade do Estado do Rio de Janeiro, Faculdade de Tecnologia, 27537-000, Resende, Rio de Janeiro, Brazil*

[3]*Instituto de Física, Universidade Federal do Rio de Janeiro, CP 68528, 21941-972, Rio de Janeiro, Rio de Janeiro, Brazil*

(Received 16 January 2023; revised 17 February 2023; accepted 24 February 2023; published 7 March 2023)

We investigate fusion reactions in collisions of neutron-halo projectiles with heavy targets. For this purpose, we use a recently developed theoretical approach to calculate cross sections for fusion processes in $^{11}\mathrm{Be} + {}^{209}\mathrm{Bi}$, $^{6}\mathrm{He} + {}^{209}\mathrm{Bi}$, and $^{6}\mathrm{He} + {}^{238}\mathrm{U}$ collisions and compare the results with the available data. The overall agreement between theory and experiment is good. Comparing the cross sections with predictions of a barrier penetration model that ignores the cluster structure of the projectile, we conclude that the fusion cross sections are suppressed above the Coulomb barrier and enhanced below. Further, we find that the deviations from predictions of the barrier penetration model depend exclusively on the breakup threshold of the projectile, increasing as it decreases.

DOI: 10.1103/PhysRevC.107.034603

I. INTRODUCTION

Nuclear reactions involving weakly bound nuclei became one of the main research topics in low energy nuclear physics [1–7]. The low binding energy affects elastic scattering and all nuclear reactions. The influence is particularly strong in collisions of projectiles far from the stability line, rich in neutrons or protons, where the breakup threshold may be lower than 1 MeV.

Fusion reactions are affected in two ways. Owing to the low breakup threshold, the nuclear density of the projectile has a long tail, leading to a lower Coulomb barrier. This *static effect* is expected to enhance fusion at all collision energies. On the other hand, the low breakup threshold strongly affects the reaction dynamics, leading to new fusion processes. First, there is the usual fusion reaction, where the whole projectile is directly absorbed by the target. This process, which also takes place in collisions of tightly bound projectiles, is usually called *direct complete fusion* (DCF). Owing to the strong breakup couplings, the projectile tends to dissociate into fragments as it approaches the target. This *dynamic* effect of the low breakup threshold hinders DCF. On the other hand, it gives rise to new fusion processes. If the target absorbs one (or more) but not all fragments, the process is called *incomplete fusion* (ICF). Of course, there is more than one ICF process, according to which particular piece of the projectile fuses with the target. Finally, there is the *sequential complete fusion* (SCF), the process where all projectile fragments fuse sequentially with the target. From the experimental point of view, DCF cannot be distinguished from SCF. Only the cross section for the sum of the two processes, called *complete fusion* (CF), can be measured.

Over the last few decades, considerable efforts have been made to determine individual CF and ICF cross sections. However, it remains a significant challenge for theorists and experimentalists. Several theoretical approaches have been proposed. Some are based on classical and semiclassical physics [8–14], and some are based on quantum mechanics within the continuum discretized coupled channel (CDCC) approximation [15–23]. Other promising models [22,24,25] are not yet in the stage of making realistic predictions for fusion cross sections of weakly bound nuclei. Recently, Lei and Moro [26] used an indirect method to determine the CF cross section for the $^{6,7}\mathrm{Li} + {}^{209}\mathrm{Bi}$ systems. They obtained it by subtracting from the total reaction cross sections the contributions of the elastic breakup, inelastic scattering, and inclusive nonelastic breakup. The latter was evaluated using the participant-spectator model of Ichimura, Austern, and Vincent (IAV) [27], whereas the cross sections for the other processes were obtained by coupled channel (CC) and CDCC calculations.

In a recent paper, we proposed a new method to calculate individual CF and ICF cross sections [20]. In this method, the cross sections are calculated in two steps. In the first, DCF and inclusive capture probabilities are evaluated through CDCC calculations. Then, the CF and ICF cross sections are obtained from these probabilities through intuitive assumptions based on classical probability theory. This method has been used to evaluate CF and ICF cross sections in collisions of the stable weakly bound $^{7}\mathrm{Li}$ [21] and $^{6}\mathrm{Li}$ [28] projectiles with heavy targets. The results were compared to the available data, and the overall agreement between the theory and the experiment was good.

Most experiments on the fusion of weakly bound projectiles can only determine the total fusion (TF) cross sections,

*jonas@if.uff.br
†jeannierangel@gmail.com
‡jlubian@id.uff.br
§canto@if.ufrj.br

which corresponds to the sum of all fusion processes. However, there are CF and ICF data for a few particular systems. Experimental CF and ICF cross sections have been measured for the stable weakly bound projectiles ^{6,7}Li [8,29–42] and ^{9}Be [29,43–53] on several heavy and medium-heavy targets. There are also fusion data for unstable weakly bound nuclei exhibiting neutron haloes. However, the number of such experiments is very small, owing to the difficulties in dealing with radioactive beams.

The first experiment on fusion of the neutron-rich nuclei was performed by Kolata *et al.* [54,55]. They measured fusion cross section in collisions of ^{6}He, a two-neutron halo nucleus, with ^{209}Bi at near-barrier energies. Comparing their data to the prediction of a barrier penetration model, the authors reported a large enhancement of fusion below the Coulomb barrier and no appreciable effect (enhancement or suppression) above it. However, it was pointed out that their findings resulted from the particular barrier penetration model (BPM) used in the comparison [56]. One would reach different conclusions by using a BPM based on a nuclear potential of a systematic approach (like the double folding model with a standard nucleon-nucleon interaction).

In 2000, Trotta *et al.* [57] measured the fusion cross section for the ^{6}He + ^{238}U system. Their experiment covered a wide energy range, reaching several MeV below the Coulomb barrier. They reported a huge enhancement at sub-barrier energies. However, a subsequent experiment by Raabe *et al.* [58], involving several authors of the previous paper, pointed out that the cross section was contaminated by fission following neutron transfer, which could be confused with fusion-fission events. They estimated this spurious contribution and corrected the previous data. Then, the resulting CF cross section showed no enhancement at sub-barrier energies. Nevertheless, owing to the extremely large error bars of the corrected data, one could not reach any conclusion about the behavior of the CF cross section at sub-barrier energies.

Other experiments on the fusion of neutron-halo nuclei were performed by Signorini *et al.* [59] and Penionzhkevich *et al.* [60]. The former studied fusion of ^{11}Be with ^{209}Bi at near-barrier energies. The latter measured fusion of the ^{6}He + ^{197}Au system at near-barrier energies. So far, the fusion of neutron-rich nuclei still needs to be satisfactorily understood. The behavior of the cross section at collision energies below and above the Coulomb barrier needs to be better established. Although it is a topic of great intrinsic interest, and plays an essential role in nucleosynthesis [61], theoretical and experimental works on this subject still need to be made available. Thus, further studies are called for.

In the present paper, we investigate fusion reactions of neutron-halo nuclei using the theoretical approach of Refs. [20,21]. We perform calculations of fusion cross sections for the ^{11}Be + ^{209}Be, ^{6}He + ^{209}Be, and ^{6}He + ^{238}U systems and compare the results to the available data. Contrasting the fusion cross sections to predictions of barrier penetration models (BPM), we investigate the influence of the low binding of the neutron halos.

The paper is organized as follows. In Sec. II, we briefly describe our theoretical approach. In Sec. III, we calculate CF and ICF cross sections for some systems and compare them to experimental data. We also present a comparative study of enhancement and suppression of fusion in the collisions studied in this work, reducing the cross sections by the fusion function method [56,62]. Finally, in Sec. IV, we present the main conclusions of our work.

II. THE THEORETICAL APPROACH

To evaluate fusion cross sections in collisions of neutron halo nuclei, we use the method of Refs. [20,21], as formulated in Ref. [28]. This method is briefly described below.

We consider fusion reactions of weakly bound light projectiles in collisions with heavy targets. The present version of our theory assumes that the projectile has a cluster structure formed by two fragments, c_1 and c_2. In a reference frame fixed at the center of the target, the position vector of the two fragments are $\mathbf{r}_1$ and $\mathbf{r}_2$, and the center of mass of the projectile is represented by $\mathbf{R}$. Denoting the relative vector between the two fragments by $\mathbf{r}$, we have the relations

$$\mathbf{r}_1 = \mathbf{R} + \frac{A_2}{A_P}\,\mathbf{r}; \quad \mathbf{r}_2 = \mathbf{R} - \frac{A_1}{A_P}\,\mathbf{r}. \tag{1}$$

Above, A_P is the mass number of the projectile while A_1 and A_2 are, respectively, the mass numbers of the fragments c_1 and c_2 ($A_P = A_1 + A_2$).

Neglecting target excitations, the collision is governed by the Hamiltonian

$$\mathbb{H}(\mathbf{R}, \mathbf{r}) = h(\mathbf{r}) + \hat{T}_{\mathbf{R}} + \mathbb{U}(\mathbf{R}, \mathbf{r}), \tag{2}$$

where $h(\mathbf{r})$ is the intrinsic Hamiltonian of the projectile within the cluster model, $\hat{T}_{\mathbf{R}}$ is the kinetic energy operator of the projectile-target relative motion, and

$$\mathbb{U}(\mathbf{R}, \mathbf{r}) = \mathbb{V}(\mathbf{R}, \mathbf{r}) - i\,\mathbb{W}(\mathbf{R}, \mathbf{r}) \tag{3}$$

is the complex potential that accounts for the collision partners' whole interaction.

The total wave function of the system for a collision with energy E, $\Psi^{(+)}(\mathbf{R}, \mathbf{r})$, satisfies the Schrödinger equation

$$\mathbb{H}(\mathbf{R}, \mathbf{r})\ \Psi^{(+)}(\mathbf{R}, \mathbf{r}) = E\ \Psi^{(+)}(\mathbf{R}, \mathbf{r}). \tag{4}$$

Usually, this equation is solved by the coupled channel method. However, collisions of weakly bound nuclei are more complicated. The difficulty is that they are strongly influenced by the continuum space of the projectile (breakup channels), leading to an infinite number of coupled equations. This problem can be handled by the CDCC method [63–65], in which the continuum is approximated by a finite set of wave functions. In the present paper, these functions are wave packets (*bins*) generated by scattering states in a $c_1 - c_2$ collision. With the discretization of the continuum, one gets a finite number of coupled equations, as in a standard coupled channel problem.

The total wave function of the system can be split into its bound (B) and continuum discretized (C) components

$$\Psi^{(+)}(\mathbf{R}, \mathbf{r}) = \Psi_B(\mathbf{R}, \mathbf{r}) + \Psi_C(\mathbf{R}, \mathbf{r}), \tag{5}$$

and one can carry out the channel expansions

$$\Psi_{\rm B}(\mathbf{R},\mathbf{r}) = \sum_{n=0}^{N_{\rm B}-1} \psi_n(\mathbf{R}) \otimes \phi_n(\mathbf{r}), \tag{6}$$

$$\Psi_{\rm C}(\mathbf{R},\mathbf{r}) = \sum_{n=N_{\rm B}}^{N-1} \psi_n(\mathbf{R}) \otimes \phi_n(\mathbf{r}). \tag{7}$$

Above, $N_{\rm B}$ and $N_{\rm C}$ are, respectively, the numbers of bound and unbound (breakup) channels in the expansions, $N = N_{\rm B} + N_{\rm C}$ is the dimension of the coupled channel space, and ϕ_n are the eigenstates of h. ϕ_0 is the ground state of the projectile, $\phi_{n=1,\ldots,N_{\rm B}-1}$ are excited bound states and $\phi_{n=N_{\rm B},\ldots,N-1}$ are CDCC bins.

Inserting the above expansion into Eq. (4) and taking the scalar product with each of the intrinsic states, one gets a set of coupled equations that can be solved by standard methods (details can be found in Ref. [20]). We performed the numerical calculations using the FRESCO code [66].

A. The projectile-target interaction

The real potential in Eq. (3) is given by the sum

$$\mathbb{V}(\mathbf{R},\mathbf{r}) = \mathbb{V}^{(1)}(\mathbf{r}_1) + \mathbb{V}^{(2)}(\mathbf{r}_2), \tag{8}$$

where $\mathbb{V}^{(i)}$ stands for the interaction between fragment c_i and the target. The expectation value of $\mathbb{V}(\mathbf{R},\mathbf{r})$ with respect to the ground state of the projectile

$$V^{00}(R) = \int d^3\mathbf{r} |\phi_0(\mathbf{r})|^2 \, \mathbb{V}(\mathbf{R},\mathbf{r}), \tag{9}$$

plays the role of the real part of the optical potential in the elastic channel. On the other hand, the off-diagonal matrix elements of $\mathbb{V}$ account for the couplings between the channels included in the expansions of Eqs. (6) and (7). Throughout this paper, we use the São Paulo potential (SPP) [67,68] for the nuclear interactions between the two clusters and the target ($\mathbb{V}^{(1)}$ and $\mathbb{V}^{(2)}$).

If the off-diagonal matrix elements of the potential are neglected, the CDCC equations reduce to a one-channel problem. In this case, the real part of the optical potential is given by Eq. (9). Owing to the long tail of $\phi_0(\mathbf{r})$, the corresponding Coulomb barrier is lower than the one associated with the SPP for the projectile-target system neglecting the cluster structure of the projectile, $V^{\rm PT}(R)$. The barriers for the two potentials are denoted respectively by $V_{\rm B}^{00}$ and $V_{\rm B}^{\rm PT}$. This feature is illustrated in Table I, which shows the barrier parameters of the two potentials for the systems studied in the present work. The barrier lowering is a static effect of the low breakup threshold, which enhances the CF cross section in the whole energy interval. It competes with the suppression arising from the breakup couplings. A detailed study of these effects will be presented in Sec. III D.

The choice of $\mathbb{W}(\mathbf{R},\mathbf{r})$ is more complicated. First, one should keep in mind that it is introduced to simulate the influence of fusion processes on the channels explicitly included in the calculations. Thus, it must be strong in the inner region of the Coulomb barriers but negligible elsewhere. Further, when acting on unbound channels, it should allow calculating

TABLE I. Barrier parameters for the potentials $V^{00}(R)$ and $V^{\rm PT}(R)$ for the systems studies in this work. The table shows also the barrier lowering, $\Delta V_{\rm B}$, arising from the low breakup threshold of each system.

target	^{6}He + ^{209}Bi	^{6}Li + ^{209}B	^{6}He + ^{238}U	^{11}Be + ^{209}Bi
$R_{\rm B}^{00}$	12.0	11.8	12.3	12.0
$V_{\rm B}^{00}$	18.6	28.2	20.1	36.3
$\hbar\omega^{00}$	3.6	4.4	3.9	3.7
$R_{\rm B}^{\rm PT}$	11.6	11.3	11.9	11.8
$V_{\rm B}^{\rm PT}$	19.4	29.8	21.0	38.2
$\hbar\omega^{\rm PT}$	4.0	4.8	4.3	4.1
$\Delta V_{\rm B}$	0.8	1.6	0.9	1.9

ICF cross sections. For this purpose, it must account for the absorption of each fragment individually. This condition is satisfied by an imaginary potential of the form

$$\mathbb{W}(\mathbf{R},\mathbf{r}) = \mathbb{W}^{(1)}(\mathbf{r}_1) + \mathbb{W}^{(2)}(\mathbf{r}_2), \tag{10}$$

where $\mathbb{W}^{(i)}$ are strong short-range potentials. In our calculations they are given by the Woods-Saxon functions

$$\mathbb{W}^{(1)}(r_i) = \frac{W_0}{1+\exp\left[(r_i - R_{\rm w})/a_{\rm w}\right]}, \tag{11}$$

where $R_{\rm w} = r_{\rm w}\left[A_i^{1/3} + A_{\rm T}^{1/3}\right]$ with the parameters $W_0 = 50\,\text{MeV}$, $r_{\rm w} = 1.0\,\text{fm}$, and $a_{\rm w} = 0.2\,\text{fm}$.

However, using this imaginary potential in the elastic channel leads to the wrong physics [28]. This becomes clear in a simplified picture, where one neglects all couplings. Then, one is left with a one-channel calculation with the optical potential given by the expectation value of Eq. (3) with respect to the g.s. of the projectile, $V^{00}(R) - i\,W^{00}(R)$. Owing to the extended tail of $\phi_0(\mathbf{r})$ (due to the low breakup threshold), $W^{00}(R)$ has a very long range, leading to strong absorption at large distances. Consequently, the fusion cross section at sub-barrier energies, arises exclusively from the action W^{00} outside the Coulomb barrier [28]. Therefore, the absorption cross section obtained this way cannot be associated with the fusion process. For this reason, $W^{00}(R)$ cannot be used to account for fusion through bound channels. Then, for these channels, we replace the potential of Eqs. (10)–(11) by

$$\mathbb{W}(\mathbf{R},\mathbf{r}) \equiv \; W^{\rm PT}(R) = \frac{W_0}{1+\exp\left[(R - R_{\rm w})/a_{\rm w}\right]}, \tag{12}$$

which is diagonal in channel space. The parameters $r_{\rm w}$ and $a_{\rm w}$ are the same as in Eq. (11), but here we use $W_0 = 100\,\text{MeV}$ [to keep the depth of $W^{00}(R)$] and $R_{\rm w} = r_{\rm w}\left[A_{\rm P}^{1/3} + A_{\rm T}^{1/3}\right]$. This potential leads to strong absorption in the inner region of the barrier, but it is negligible around the barrier radius and beyond it.

B. The fusion cross sections

The method of Refs. [20,21,28] assumes that bound channels contribute exclusively to DCF whereas unbound channels contribute to fusion processes following breakup. That is, ICF1, ICF2, and SCF. Using a standard expression for

absorption cross sections [69], one obtains [28]

$$\sigma_{\rm DCF} = \frac{1}{|\mathcal{A}|^2}\,\frac{K}{E}\,\langle\Psi_{\rm B}|W^{\rm PT}|\Psi_{\rm B}\rangle, \tag{13}$$

$$\sigma_{\rm F}^{(1)} = \frac{1}{|\mathcal{A}|^2}\,\frac{K}{E}\,\langle\Psi_{\rm C}|\mathbb{W}^{(1)}|\Psi_{\rm C}\rangle, \tag{14}$$

$$\sigma_{\rm F}^{(2)} = \frac{1}{|\mathcal{A}|^2}\,\frac{K}{E}\,\langle\Psi_{\rm C}|\mathbb{W}^{(2)}|\Psi_{\rm C}\rangle, \tag{15}$$

where K is the wave number corresponding to the energy E, and $\mathcal{A}$ is the normalization constant of the scattering wave function. Above, $\sigma_{\rm DCF}$ is the cross section for DCF, and the other two are inclusive cross sections to capture one of the fragments. That is, cross sections for the fusion of one fragment with the target, independently of what happens to the other.

Note that Eqs. (13), (14), and (15) involve off-diagonal matrix-elements of the imaginary potentials, but only within the subspace associated with the cross section. That is, B in the case of $\sigma_{\rm DCF}$, and C in the cases of $\sigma_{\rm F}^{(1)}$ and $\sigma_{\rm F}^{(2)}$. This can be seen more clearly if one replaces $\Psi_{\rm B}$ and $\Psi_{\rm C}$ by the channel expansions of Eqs. (6) and (7). On the other hand, these expressions do not include matrix elements between channels in different subspaces. The theoretical model assumes that matrix elements of the imaginary potentials between channels in different subspaces are negligible [20].

By carrying out angular momentum projections, the above expressions can be put in the form

$$\sigma_{\rm DCF} = \frac{\pi}{K^2}\sum_J (2J+1)\,\mathcal{P}^{\rm DCF}(J), \tag{16}$$

$$\sigma_{\rm F}^{(1)} = \frac{\pi}{K^2}\sum_J (2J+1)\,\mathcal{P}^{(1)}(J), \tag{17}$$

$$\sigma_{\rm F}^{(2)} = \frac{\pi}{K^2}\sum_J (2J+1)\,\mathcal{P}^{(2)}(J), \tag{18}$$

where $\mathcal{P}^{\rm DCF}(J)$, $\mathcal{P}^{(1)}(J)$, and $\mathcal{P}^{(2)}(J)$ are, respectively, the probabilities of DCF, and of the inclusive captures of c_1 and c_2, in a collision with total angular momentum J. Expressions for these probabilities can be found in the Appendix of Ref. [21].

We remark that the above expressions are based on full quantum mechanics within the CDCC approximation.

CF and ICF

The fusion cross sections of Eqs. (16)–(18) alone are not very useful since they cannot be directly compared to the CF and ICF data when they are available. Experimental CF cross sections are sums of the DCF and SCF, and experimental ICF cross sections correspond to exclusive events where one of the fragments is captured by the target while the other is not. Then, to make predictions of observable cross sections, one has to make further assumptions.

We use classical probability theory to relate the cross sections of Eqs. (16)–(18) to the observed CF, ICF1, and ICF2 cross sections. Following Ref. [28], the ICF1, ICF2, and SCF probabilities are related to the probabilities of Eqs. (16)–(18) through the equations

$$\mathcal{P}^{\rm ICF1}(J) = \mathcal{P}^{(1)}(J)\times[1-\mathcal{P}^{(2)}(J)], \tag{19}$$

$$\mathcal{P}^{\rm ICF2}(J) = \mathcal{P}^{(2)}(J)\times[1-\mathcal{P}^{(1)}(J)], \tag{20}$$

$$\mathcal{P}^{\rm SCF}(J) = \mathcal{P}^{(1)}(J)\times\mathcal{P}^{(2)}(J), \tag{21}$$

and the corresponding cross sections are

$$\sigma_{\rm SCF} = \frac{\pi}{K^2}\sum_J (2J+1)\,\mathcal{P}^{\rm SCF}(J), \tag{22}$$

$$\sigma_{\rm ICF1} = \frac{\pi}{K^2}\sum_J (2J+1)\,\mathcal{P}^{\rm ICF1}(J), \tag{23}$$

$$\sigma_{\rm ICF2} = \frac{\pi}{K^2}\sum_J (2J+1)\,\mathcal{P}^{\rm ICF2}(J). \tag{24}$$

Then, one gets the observed cross sections

$$\sigma_{\rm CF} = \sigma_{\rm DCF} + \sigma_{\rm SCF}, \tag{25}$$

$$\sigma_{\rm ICF} = \sigma_{\rm ICF1} + \sigma_{\rm ICF2}, \tag{26}$$

$$\sigma_{\rm TF} = \sigma_{\rm CF} + \sigma_{\rm ICF}. \tag{27}$$

C. Fusion functions

In Sec. III, we will use the theory of the previous section to calculate fusion cross sections for different systems attempting to find general trends of the fusion processes. However, comparisons of cross sections for different systems are only meaningful if one first eliminates the influence of trivial properties of the system, like the height and radius of the Coulomb barrier. This can be achieved by reducing the fusion cross sections (a discussion of the reduction methods available in the literature can be found in Ref. [70]). We use the fusion function (FF) reduction method [56,62], which is briefly described below. In this method, the collision energy and the cross section are respectively transformed into the dimensionless variables x and $F(x)$, according to the relations

$$x = \frac{E_{\rm c.m.}-V_{\rm B}}{\hbar\omega} \quad\text{and}\quad F(x) = \frac{2E_{\rm c.m.}}{\hbar\omega R_{\rm B}^2}\,\sigma. \tag{28}$$

The system dependence of the cross section is completely eliminated if it can be approximated by the Wong formula [71]

$$\sigma_{\rm F}^{\rm (W)} = R_{\rm B}^2\,\frac{\hbar\omega}{2E}\,\ln\left[1+\exp\left\{\frac{2\pi(E-V_{\rm B})}{\hbar\omega}\right\}\right]. \tag{29}$$

In this case, inserting this expression into Eq. (28), one gets the universal fusion function (UFF)

$$F_0(x) = \ln[1+\exp(2\pi x)]. \tag{30}$$

In typical situations, the fusion cross section is influenced by the intrinsic structure of the collision partners, so the Wong formula cannot approximate it. Then the corresponding fusion function deviates from the UFF. In this way, $F_0(x)$ can be considered a benchmark to assess the influence of particular nuclear properties. It is well known that fusion functions associated with the CF of weakly bound systems at above-barrier energies are suppressed concerning the UFF (for a detailed discussion, see, e.g., Ref. [4]). Usually, this effect is measured

by a suppression factor, which is related to the strength of the breakup couplings.

However, one should keep in mind that the fusion function method is based on the assumption that the Wong formula ($\sigma_{\rm W}$) is a good approximation to the BPM cross section ($\sigma_{\rm BPM}$). This approximation is very good for heavy systems where $Z_P\,Z_T > 500$ (see Ref. [56]). For lighter systems, it may overestimate the BPM cross section at sub-barrier energies badly. Nevertheless, this problem can be fixed if one replaces the fusion functions with their renormalized versions, given by the relation [56,62]

$$\overline{F}(x) = F(x) \times \frac{\sigma_{\rm W}}{\sigma_{\rm BPM}}. \tag{31}$$

For the systems studied in the present work, the products of atomic numbers are in the range $332 \geqslant Z_P\,Z_T \geqslant 166$. Thus, the comparisons of Sec. III D must be based on the renormalized fusion function of Eq. (31).

III. APPLICATIONS

Now we use the theory of the previous section to study collisions of the one-neutron halo nucleus ^{11}Be and the two-neutron halo nucleus ^{6}He. We consider the systems: $^{11}\mathrm{Be} + {}^{209}\mathrm{Bi}$, $^{6}\mathrm{He} + {}^{209}\mathrm{Bi}$, and $^{6}\mathrm{He} + {}^{238}\mathrm{U}$. As mentioned in the introduction, there are also available data for the $^{6}\mathrm{He} + {}^{197}\mathrm{Au}$ system [60]. However, in this experiment, the error bars associated with the collision energies and the cross sections are extremely large. Then, comparing our model's predictions with this data set would lead to no reliable conclusion. For this reason, we will not consider this system in the present paper.

In comparing theoretical and experimental CF cross sections, one should keep in mind that theorists and experimentalists may adopt different definitions of CF. From the theoretical point of view, CF is the process where the whole projectile (all nucleons) fuses with the target. From the experimental point of view, any process where the full charge of the projectile is captured by the target, independently of what happens to its neutrons, is frequently considered CF. The two definitions coincide when the projectile breaks up into two charged fragments, like ^{6}Li ($^{6}\mathrm{Li} \rightarrow {}^{4}\mathrm{He} + {}^{2}\mathrm{H}$). However, they differ in collisions of neutron halo nuclei, like ^{6}He ($^{6}\mathrm{He} \rightarrow {}^{4}\mathrm{He} + 2n$). In this case, only the ^{4}He fragment is charged. Then, the CF data correspond to ^{6}He fusion but it may also have contributions from the capture of the ^{4}He fragment following the breakup. In such cases, the experimental fusion data should be compared with the sum of the theoretical CF and ICF2 cross sections.

A. ^{11}Be + ^{209}Bi

1. Intrinsic states and continuum discretization

^{11}Be is a weakly bound nucleus with cluster configuration. It is formed by a ^{10}Be core (c_2) surrounded by a halo of one neutron (c_1) bound by 0.5 MeV. Owing to the low binding, collisions of ^{11}Be are strongly influenced by the breakup channel ($^{11}\mathrm{Be} \rightarrow {}^{10}\mathrm{Be} + n$). From the theoretical point of view, $^{11}\mathrm{Be} + {}^{209}\mathrm{Bi}$ scattering can be treated by the three-body CDCC method [63–65].

The relative $c_1 - c_2$ motion is governed by the intrinsic Hamiltonian

$$h(\mathbf{r}) = -\frac{\hbar^2}{2\mu_{12}}\nabla^2_{\mathbf{r}} + v_{12}(r), \tag{32}$$

where $\mu_{12} = m_0 A_1 A_2/(A_1 + A_2)$, with A_1 and A_2 standing for the mass numbers of c_1 and c_2 ($A_1 = 1$ and $A_2 = 10$ in the present case), and m_0 is the nucleon mass. In Eq. (32), $v_{12}(r)$ is the interaction between the two clusters, which is parameterized by a Woods-Saxon function and its derivative (for the spin-orbit term).

As is frequently done in CDCC calculations, different parameters were used to describe bound and unbound (CDCC bins) states of the projectile. We have adopted the parameters of di Pietro *et al.* [72] based on the paper of Capel *et al.* [73]. The radius and diffusivity parameters and the strength of the spin-orbit term were fixed. The depth of the volumetric part of the potential for even parity was adjusted to give the correct binding energy (BE) of the ground state of this nucleus. This potential also correctly describes the resonant state ($J^\pi = 5/2^+$, $\varepsilon_{\rm res} = 1.28\,$MeV, $\Gamma_{\rm res} = 100\,$keV).

Our CDCC calculations included bins with orbital angular momenta up to $l_{\rm max} = 4\hbar$, and we took into account coupling matrix elements with multipolarities up to $\lambda_{\rm max} = 5$. The continuum was truncated at the energy $\varepsilon_{\rm max} \simeq 8\,$MeV. For nonresonant angular momenta ($l \neq 2$), we used four bins with the constant width, $\Delta\varepsilon = 2\,$MeV. For $l = 2$, we used a sharper mesh in the resonance region. Below the resonance energy, we set two bins of 0.5 MeV (from 0 to 1.0 MeV). These bins were followed by a bin of 0.4 MeV containing the resonance energy, going from 1.0 to 1.4 MeV. The remaining part of the [0–8] MeV interval was covered by five bins of equal widths ($\Delta\varepsilon \approx 1.3\,$MeV). The continuum discretization described above leads to very good convergence of the calculated fusion cross sections. We point out that continuum discretization in the presence of sharp resonances deserves particular attention. In the neighbourhood of a sharp resonance, the phase-shift approaches $\pi/2$ very fast. Then, the scattering states generating the bins change rapidly, leading to numerical instabilities. To avoid this problem, the FRESCO code gives special treatment to the bin, including the resonance energy. The usual normalization factor, $\exp[-i\delta(k)]$, is multiplied by the extra factor $\sin[\delta(k)]$.

As we pointed out in our previous papers [21,28], we use the cluster model to calculate bound states of the projectile. Although the cluster configuration is expected to be a large component of these states, its amplitude is not equal to one. To fix the problem, one should multiply the matrix elements between bound states and bins by some spectroscopic amplitude, $\mathcal{S}$. This amplitude, which needs to be better determined, is expected to be of the order of one, but not exactly one. The value adopted for each system will be discussed below.

2. The CF cross section

The collision dynamics in $^{11}\mathrm{Be} + {}^{209}\mathrm{Bi}$ scattering is strongly affected by breakup couplings, which are dominated

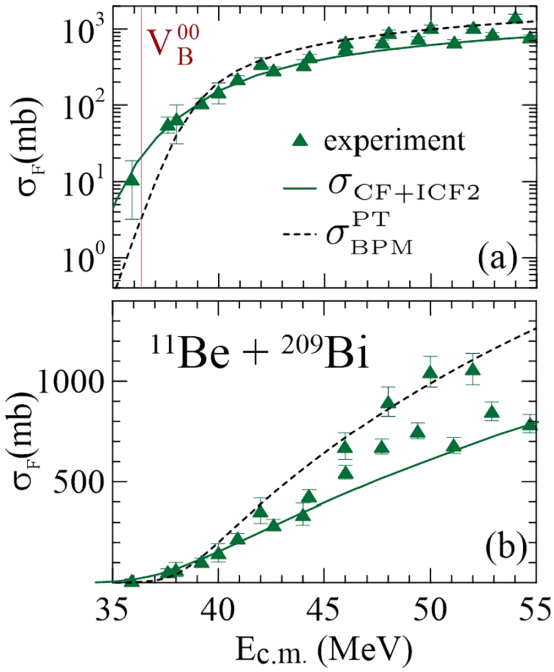

FIG. 1. Experimental fusion cross section for the $^{11}\mathrm{Be} + {}^{209}\mathrm{Bi}$ system [59], in comparison with the prediction of our model and of the BPM. See the text for details.

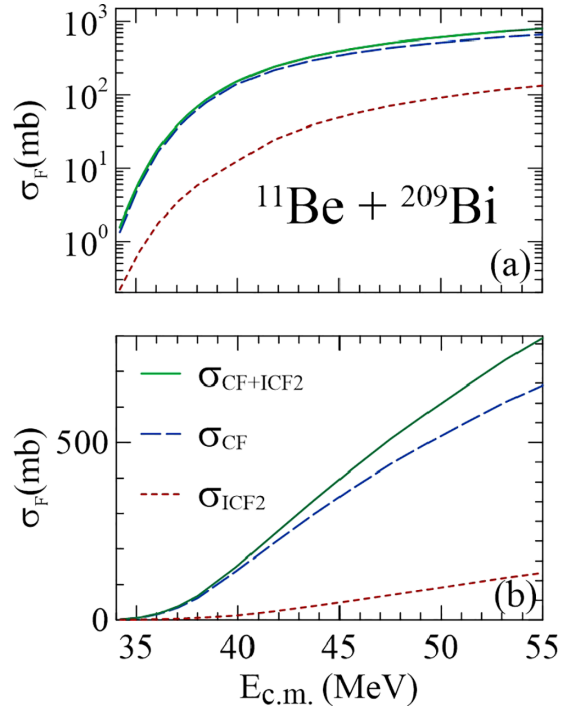

FIG. 2. The theoretical cross section σ_F [Eqs. (16), (22), and (25)] for the $^{11}\mathrm{Be} + {}^{209}\mathrm{Bi}$ system, and its CF and ICF_2 components. For details see the text.

by the Coulomb dipole term. The experimental $B(E1)$ for the transition between the g.s. of ^{11}Be to its bound excited state is $B(E1)_{\rm exp} = 0.115\, e^2\,\mathrm{fm}^2$ [72], whereas the value obtained by the cluster model is $B(E1)_{\rm calc} = 0.261\, e^2\,\mathrm{fm}^2$. Then, we infer that the spectroscopic amplitude can be approximated by

$$\mathcal{S} \simeq \sqrt{B(E1)_{\rm exp}/B(E1)_{\rm calc}} = 0.66.$$

We compare the data of Signorini *et al.* [59] with the results of our calculations, setting $\mathcal{S} = 0.66$. The experiment determined the fusion cross section by detecting characteristic alpha particles and fission fragments emitted by the fusion evaporation residues. However, the same evaporation residues are produced by the fusion of ^{11}Be and by the capture of the ^{10}Be fragment following the breakup of the projectile. Thus, the data actually correspond to the sum of cross sections for the CF and ICF2 (capture of ^{10}Be) fusion processes. Then, for consistency, one should compare the data to the calculated cross section

$$\sigma_{\rm CF+ICF2} = \sigma_{\rm CF} + \sigma_{\rm ICF2}. \tag{33}$$

Figure 1 shows the fusion data of Ref. [59] compared to two theoretical cross sections: $\sigma_{\rm CF+ICF2}$ and $\sigma_{\rm BPM}^{\rm PT}$. The former is the cross section Eq. (33). The latter is the prediction of the barrier penetration model (BPM) for the São Paulo potential neglecting the cluster structure of the projectile, denoted by $V^{\rm PT}(R)$. The results are shown in logarithmic [Fig. 1(a)] and linear [Fig. 1(b)] scales. Around and below the Coulomb barrier, the predictions of our model are in very good agreement with the data. However, above 45 MeV, the agreement is much worse. The data exhibit large fluctuations as the energy increases. They are spread between the lines representing $\sigma_{\rm BPM}^{\rm PT}$ and $\sigma_{\rm CF+ICF2}$. Although the data are clearly suppressed with respect to $\sigma_{\rm BPM}$, it is impossible to estimate a suppression factor from this data set.

Although the experiment of Ref. [59] could not distinguish $\sigma_{\rm CF}$ from $\sigma_{\rm ICF2}$, the authors claim that the contribution of the latter is small, not exceeding 30% of the former. Since our model leads to individual cross sections for the two fusion processes, we can check if they are consistent with this statement. Figure 2 shows the theoretical cross sections $\sigma_{\rm CF}$, $\sigma_{\rm ICF2}$, and $\sigma_{\rm CF+ICF2}$. Indeed, $\sigma_{\rm ICF2}$ is much smaller than $\sigma_{\rm CF}$. At the highest energies, where the relative importance of $\sigma_{\rm ICF2}$ is maximal, it is about 20% of $\sigma_{\rm CF}$. We conclude that the relative importance of the two fusion processes agrees with the findings of Refs. [59,74].

B. $^{6}\mathrm{He} + {}^{209}\mathrm{Bi}$

1. Intrinsic states and continuum discretization

The ^{6}He projectile has a strong cluster structure consisting of an α particle plus a halo of two neutrons. The projectile breaks up into three fragments, as $^{6}\mathrm{He} \rightarrow {}^{4}\mathrm{He} + n + n$, with the breakup threshold $B = 0.97\,\mathrm{MeV}$. Then, the ideal treatment of the collision would be through the four-body CDCC approach, where the intrinsic states of the projectile are complicated three-body wave functions [17,75–78]. However, Moro *et al.* [76] have shown that the right rms radius of ^{6}He and good descriptions of elastic scattering data in collisions of this nucleus with a heavy target can be achieved by approximating the two valence neutron by a single particle, the *dineutron*, provided that one uses an effective breakup thresh-

old of $B = 1.6$ MeV. This approximation greatly simplifies the problem since the simpler three-body CDCC can treat the collision.

Following Moro *et al.* [76], we used the same WS nuclear potential for the g.s. of ^{6}He (its only bound state) and scattering states with $l \neq 2\hbar$. The parameters of the potential were determined by fitting the effective separation energy of 1.6 MeV. For $l = 2\hbar$, the depth of the potential was modified by fitting the energy of the sharp 2^+ resonance at $\varepsilon_{res} = 197$ keV. The details of these potentials can be found in Ref. [76].

In our CDCC calculations, we considered bound and unbound states of the projectile with angular momentum up to $l_{max} = 2\hbar$ and truncated the continuum at $\varepsilon_{max} = 8$ MeV. We considered coupling matrix elements with multipolarities up to $\lambda_{max} = 4\hbar$. In the absence of resonances ($l \neq 2\hbar$), the continuum was split into three intervals. The first, ranging from $\varepsilon = 0$ to $\varepsilon = 2$ MeV, was discretized by ten bins with width $\Gamma = 0.2$ MeV. The next, from 2 to 4 MeV, was covered by two bins with width $\Gamma = 1$ MeV. The last interval, ranging from 4 to 8 MeV, was discretized by two bins with $\Gamma = 2$ MeV. For $l = 2$ we used a sharper mesh in the resonance region. Below the resonance energy, we set a thin bin, going from $\varepsilon = 0$ to $\varepsilon = 0.1$ MeV, followed by the resonant bin, from $\varepsilon = 0.1$ to 0.2 MeV. These bins were followed by nine bins of width $\Gamma = 0.2$ MeV, covering the region between $\varepsilon = 0.2$ to $\varepsilon = 2$ MeV. To discretize the continuum between $\varepsilon = 2$ to $\varepsilon = 8$ MeV, we used the same procedures adopted for $l \neq 2\hbar$.

With the treatment of the continuum described above, we got very good convergence of the calculated fusion cross sections.

2. The CF cross section

Kolata *et al.* [54,55] measured fusion cross sections in ^{6}He + ^{209}Bi collisions at near-barrier energies. CF of this system leads to the formation of ^{215}At, which evaporates neutrons, forming lighter At isotopes. PACE calculations in the energy range of the experiment indicate that ^{215}At decays exclusively by evaporation of two, three, and four neutrons, forming respectively ^{213}At, ^{212}At, and ^{211}At. Further, these calculations indicated that the contribution from ^{213}At are only relevant at energies well below the Coulomb barrier. Then, they were neglected. The fusion cross section was then determined by measurements of the characteristic alpha particles emitted in the decays of ^{212}At and ^{211}At.

On the other hand, ICF leads to ^{213}At, which forms ^{212}At and ^{211}At through the evaporation of one and two neutrons, respectively. We can discard contributions from ^{213}At to the data because they were not measured in this experiment. However, some of the detected alpha particles could result from ICF events. To investigate this possibility, we consider the excitation energies of the ^{212}At and ^{211}At nuclei formed in the ICF chain. The Q value of the ^{4}He + ^{209}Bi $\rightarrow$ ^{212}At + n reaction has the highly negative value of $Q = -15$ MeV. The highest beam energy (converted to the c.m. frame) in the experiment is 29 MeV. Subtracting the energy to break ^{6}He up, $\approx$1 MeV, there is 28 MeV to be shared by the alpha particle and the neutrons. In the most favorable situation, where the fragments have roughly the velocity as the incident beam, the α particle carries 2/3 of the incident energy, namely $\approx$19 MeV. Then, most experimental points are below the threshold of ^{212}At formation. The formation of ^{211}At is still more unlikely, as in this case, the Q value is -19 MeV. Then, it is reasonable to assume that the data of this experiment correspond, basically, to CF, although the data points at the highest energies could have some contribution from ICF.

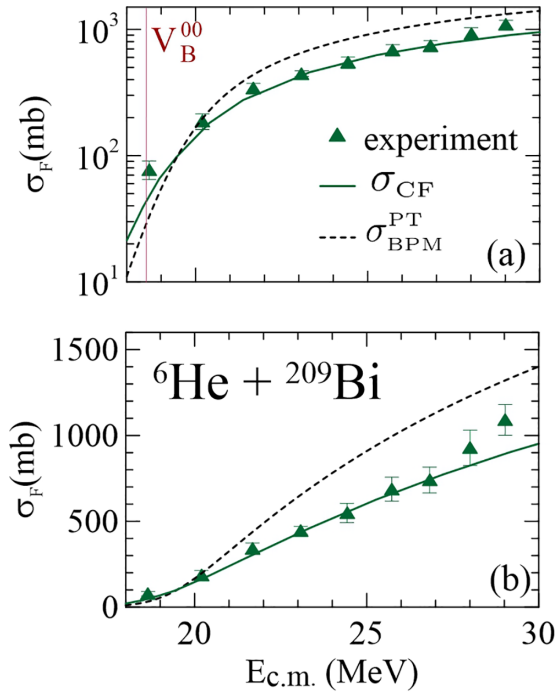

FIG. 3. Experimental CF cross section for the ^{6}He + ^{209}Bi system [54,55]. The figure shows also the theoretical CF cross section of our model, σ_{CF}, and that of the BPM with the potential $V^{PT}(R)$, σ_{BPM}^{PT}. See the text for further details.

Figure 3 shows the data of Kolata *et al.* [54,55], together with the CF cross section of our model, σ_{CF}. In our calculations, we used the spectroscopic amplitude $\mathcal{S} = 0.7$ (the same value adopted for ^{6}Li in collisions with the same target [28]). For comparison, we also show the cross section predicted by the BPM neglecting the cluster structure of the projectile, σ_{BPM}^{PT}. All cross sections are shown in logarithmic [Fig. 3(a)] and linear [Fig. 3(b)] scales.

Inspecting Fig. 3, one concludes that our model describes the data very well, although the theoretical curve is slightly below the lowest energy data point. It also underpredicts the data at the highest energies of the experiment. This might indicate a contribution from ICF, as discussed earlier in this section. On the other hand, comparing the data to σ_{BPM}^{PT}, we find that the experimental cross section is suppressed above the barrier and enhanced below it. The suppression is due to couplings with breakup channels, whereas the enhancement is due to the reduction of the Coulomb barrier, arising from the low breakup threshold, $\Delta V_B \equiv V_B^{PT} - V_B^{00} = 0.8$ MeV (see Table I). This point will be further discussed in Sec. III D.

Comparing CF suppressions in collisions of ^{6}He and ^{6}Li (a stable weakly bound isobar of ^{6}He) with the same ^{209}Bi target nucleus is interesting. For this purpose, we reduce the

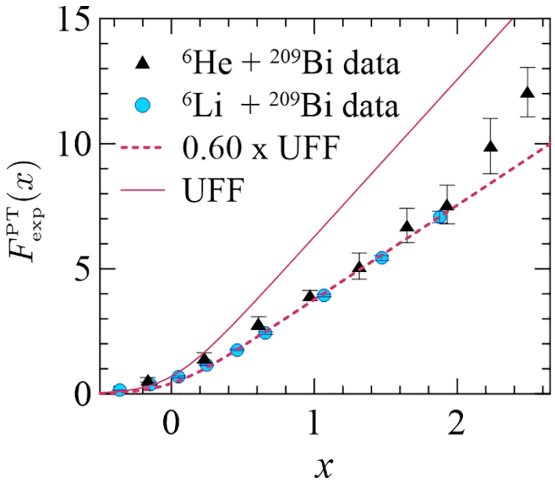

FIG. 4. Fusion functions in collisions of ^{6}He and ^{6}Li projectiles on a ^{209}Bi target, corresponding to the data of Refs. [54,55] and [8,29], respectively, based on the parameters of $V^{PT}(R)$. See the text for details.

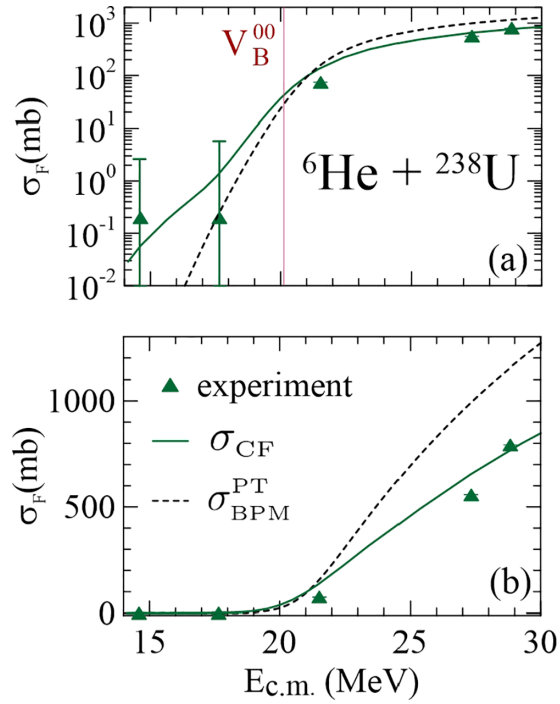

FIG. 5. Experimental CF section for the ^{6}He + ^{238}U system [58], in comparison with the prediction of our model. The BPM cross section for the potential $V^{PT}(r)$ is also shown. See the text for details.

experimental CF cross sections of Refs. [54,55] and [8,29] by the fusion function method. We evaluated fusion functions through Eq. (28), using the barrier parameters of the potential $V^{PT}(r)$ (see Table I). These fusion functions are denoted by $F_{exp}^{PT}(x)$. The results are shown in Fig. 4.

One finds that the experimental fusion functions for the two systems are very similar and appreciably lower than the UFF. They closely follow the trend of the red dashed line, which represents the UFF multiplied by the factor 0.60, except for the two data points for ^{6}He at the highest energies, which are somewhat higher. Thus, the CF cross sections for the two systems are suppressed by ≈40%.

C. ^{6}He + ^{238}U

The intrinsic states and the details of the continuum discretization for this system are identical to those of the ^{6}He + ^{209}Bi system.

1. Fusion cross sections

The fusion cross section for this system at sub- and near-barrier energies has been measured by Trotta *et al.* [57]. They found a huge enhancement at sub-barrier energies. In this experiment, the signature of fusion events was the detection of two fission fragments emitted back to back, unaccompanied by a third charged fragment with a projectile-like kinematic. CF leads to the formation of a highly excited ^{244}Pu CN. Since the excitation energy is well above the fission barrier, it decays exclusively by fission. On the other hand, fusion of the ^{4}He fragment with ^{238}U is a highly endothermic reaction, so that the excitation energy of the resulting ^{242}Pu CN is well below the fission barrier. Then, it decays through other modes that were not measured in this experiment. For this reason, the authors of the experiment argue that their data correspond exclusively to CF.

However, a subsequent experiment of the same group [58] led to the conclusion that the large CF cross sections at sub-barrier energies were mainly due to the contribution of fission following two-neutron transfer, which were not fully discarded. This contribution was estimated by DWBA calculations and was subtracted from the fission cross section. The CF cross section obtained through this procedure did not confirm the very large enhancement found in the previous experiment.

Figure 5 shows the data of Raabe *et al.* [58] in comparison with the predictions of our model. The cross section, $\sigma_{BPM}^{PT}(E)$ is also shown. Above the Coulomb barrier ($E_{c.m.} > 21$ MeV), one observes that the data are very well described by our model and that it is suppressed with respect to σ_{BPM}^{PT}. At $E_{c.m.} = 30$ MeV, the ratio of the two cross sections is about ≈0.6. Below the Coulomb barrier, the predictions of our model are enhanced with respect to σ_{BPM}^{PT}, and they are consistent with the data. Nevertheless, the agreement between theory and experiment in this energy region is not meaningful, owing to the large error bars of the CF data. The lowest data points, several MeV below the barrier, have error bars about one order of magnitude larger than the data. Although one cannot learn much from this comparison, it called our attention to the abrupt change in the slope of σ_{CF} between 17 and 18 MeV (a few MeV below the Coulomb barrier). The origin of this change is addressed below.

2. The low energy behavior of CF

According to Eq. (25), the CF cross section is the sum of the DCF and SCF components. The former are the contributions from bound channels, whereas the latter arises from the continuum. As the energy decreases well below the Coulomb barrier, the influence of breakup couplings becomes very

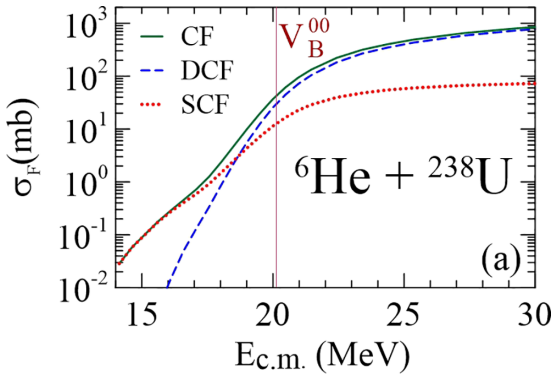

FIG. 6. The CF fusion cross section for the ^{6}He + ^{238}U system, together with its direct and sequential components.

weak, and the population of the continuum becomes very small. Then, one might be led to conclude that the CF cross section would be dominated by $\sigma_{\rm DCF}$. However, one should keep in mind that sub-barrier fusion involves transmission coefficients that become vanishingly small well below the Coulomb barrier. Further, these coefficients strongly depend on the reduced mass, decreasing rapidly as it increases. In this way, the transmission coefficient for the whole projectile, involved in DCF, could be much lower than the ones for the clusters involved in ICF and SCF. The situation is particularly favorable in the SCF of ^{6}He since there is no Coulomb barrier for the dineutron.

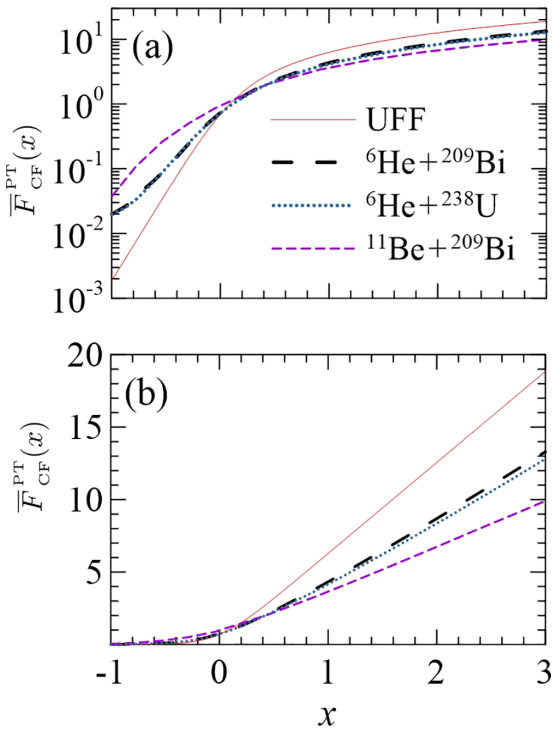

FIG. 7. Renormalized fusion functions associated with the CF cross section of our model, evaluated with the barrier parameters $R_{\rm B}^{\rm PT}$, $V_{\rm B}^{\rm PT}$, and $\hbar\omega^{\rm PT}$. See the text for details.

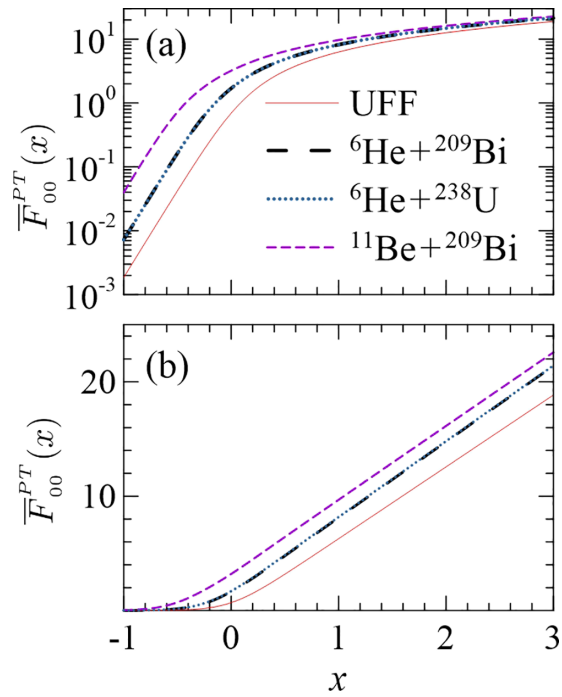

FIG. 8. Renormalized fusion functions for $\sigma^{00}_{\rm BPM}(E)$, evaluated with the barrier parameters $V^{\rm PT}(r)$.

To clarify the situation, Fig. 6 shows the CF cross section of the previous figure, together with its DCF and SCF components. One observes that the contribution from the latter is small at above-barrier energies, less than 10% at $E_{\rm c.m.} \approx 30$ MeV. On the other hand, it is the dominant component below ≈18.5 MeV, becoming more than one order of magnitude larger at 16 MeV. Note that a similar situation would be found for the ^{6}He + ^{209}Bi system. The change of slope in the CF cross section has not been observed in Fig. 3 because the energy range of the figure was restricted to the energies of the experiment. This will be shown in the next section.

D. Comparative study of CF

As we mentioned earlier, the low breakup threshold of ^{11}Be and ^{6}He affect the CF cross sections in two ways. First, the low binding of the fragments leads to a reduction of the Coulomb barrier. That is, $V_{\rm B}^{00} < V_{\rm B}^{\rm PT}$ (see Table I). This leads to an enhancement of the fusion cross section at all collision energies. On the other hand, the low breakup threshold of the projectile makes breakup couplings very important, transferring an appreciable part of the incident flux to breakup channels. This dynamic effect is expected to suppress the CF cross section.

In this section, we carry out a comparative study of these effects in the ^{11}Be + ^{209}Bi, ^{6}He + ^{209}Bi, and ^{6}He + ^{238}U systems. However, a study of this kind must be based on something other than the fusion cross sections as they are. One should first reduce them to eliminate the influence of charges and sizes of the collision partners. We achieve this goal using the fusion function method (see Sec. II C). Further, since the systems considered here are not heavy enough, we

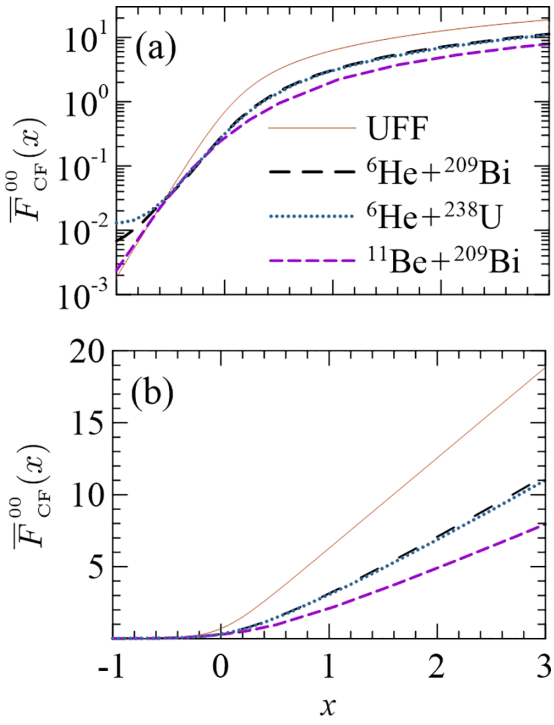

FIG. 9. Renormalized fusion functions associated with the CF cross section of our model, evaluated with the barrier parameters R_B^{00}, V_B^{00}, and $\hbar\omega^{00}$. See the text for details.

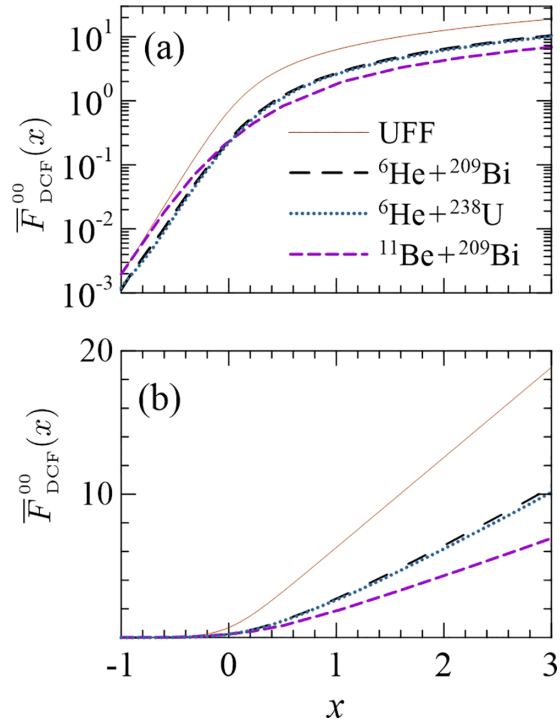

FIG. 10. Same as the previous figure, but considering only the direct component of the CF cross section.

use the renormalized fusion function of Eq. (31) rather than its original form [Eq. (28)].

We begin by assessing the net effect of the low breakup threshold on σ_{CF}. Figure 7 shows renormalized fusion functions for the ^{11}Be + ^{209}Bi, ^{6}He + ^{209}Bi, and ^{6}He + ^{238}U systems compared to the UFF. To keep both the static and the dynamic effects of the low breakup threshold, the fusion functions were evaluated with the barrier parameters R_B^{PT}, V_B^{PT}, and $\hbar\omega^{PT}$. They are denoted by $\overline{F}^{PT}_{CF}(x)$. Comparing them to the UFF, one finds the same qualitative behavior: enhancement below the Coulomb barrier and suppression at above-barrier energies. Further, one observes that the deviations from the UFF depend exclusively on the breakup threshold of the projectile, at least for targets in the same mass range. In collisions of ^{6}He with the two heavy targets, the fusion functions are extremely close, and in the case of the ^{11}Be projectile, which has a lower breakup threshold, the deviations from the UFF are more pronounced.

One can also investigate the static or dynamic effect individually. To isolate the influence of the barrier lowering, we switch off channel couplings in our CDCC calculations. Then, it reduces to a one-channel calculation with the real potential $V^{00}(R)$ plus the short-range imaginary potential $W^{PT}(R)$. The resulting cross section is essentially the one of the barrier penetration model for $V^{00}(R)$, denoted by σ^{00}_{BPM}. Next, we evaluate renormalized fusion functions associated with this cross section, using the barrier parameters of $V^{PT}(r)$. These fusion functions, denoted by $\overline{F}^{PT}_{00}(x)$, are shown in Fig. 8, together with the UFF. As expected, one observes that they are enhanced at all energies. Further, the enhancement increases with the strength of the barrier lowering, ΔV_B (see Table I), which is strongly correlated with the breakup threshold. It increases as the breakup threshold decreases. Thus, the strongest enhancement is found in the case of ^{11}Be, which has the lowest breakup threshold. The two fusion functions can hardly be distinguished in collisions of ^{6}He with ^{209}Bi and ^{238}U.

We can also study the influence of breakup couplings alone, eliminating the influence of the barrier lowering, ΔV_B. Although we cannot switch off ΔV_B, we can suppress its effects on the renormalized fusion functions by evaluating them with $V^{00}(R)$ parameters, namely R_B^{00}, V_B^{00}, and $\hbar\omega^{00}$. These fusion functions, denoted by $\overline{F}^{00}_{CF}(x)$, are shown in Fig. 9. Above the Coulomb barrier, they are all suppressed with respect to the UFF, and the strength of the suppression increases as the breakup threshold decreases. The two curves for ^{6}He projectiles are very close, with the fusion function for ^{238}U being slightly lower. This is a consequence of the larger charge of ^{238}U, which leads to slightly stronger breakup couplings. In principle, one would expect that the breakup couplings would lead to CF suppression at all collision energies. However, it is not so. For $x \lesssim -0.5$, the fusion functions are larger than the UFF, especially the one for the ^{6}He + ^{238}U system. The reason for this unexpected behavior is the contribution from SCF. As we pointed out in the discussion of Fig. 6, sequential complete fusion becomes dominant a few MeV below the Coulomb barrier, and this reaction mechanism does not follow the same trend as the DCF component. In particular, the renormalization of the fusion function is not appropriate for SCF.

To show more clearly that SCF is responsible for the unexpected low-energy behavior of the fusion functions, we

present a new version of Fig. 9, considering only the DCF component of the CF cross section. The resulting fusion functions, denoted by $\overline{F}^{00}_{\rm DCF}(x)$, are shown in Fig. 10. Since above the Coulomb barrier, the contribution from SCF to $\sigma_{\rm CF}$ is very small, Figs. 9 and 10 are quite similar. However, at sub-barrier energies, they are very different. In Fig 10, the fusion functions are always below the UFF, approaching it asymptotically as the energy decreases.

IV. CONCLUSIONS

We presented a study of fusion reactions in collisions of neutron-halo projectiles with heavy targets. We used a recently developed theory to evaluate complete and incomplete fusion for the ^{6}He + ^{209}Bi, ^{6}He + ^{238}U, and ^{11}Be + ^{209}Bi systems and compared the results with the available data. The main conclusions of the present work are summarized below.

(1) Our theory describes fairly well the complete (or complete + incomplete) fusion data in collisions of neutron halo nuclei.
(2) Comparing the cross sections of our model with predictions of the barrier penetration model with the São Paulo potential, we found that the overall effect of the low breakup threshold is enhancement at sub-barrier energies and suppression above the Coulomb barrier (of ≈40% in the collision of ^{11}Be with ^{209}Bi, and of ≈30% in collisions of ^{6}He with the ^{209}Bi and ^{209}Bi targets).
(3) We found that the theoretical CF cross sections in ^{6}He collisions at energies well below the Coulomb barrier exhibits a sudden change in its slope. This change was traced back to the contribution of sequential complete fusion. This fusion process becomes dominant in this energy region, owing to the lack of a Coulomb barrier to the neutrons. This behavior could not be checked in the ^{6}He + ^{238}U data due to the large error bars at sub-barrier energies. It would be interesting to check this feature in new experiments.
(4) We investigated the static and dynamic effects of the low breakup threshold in the three systems considered in this work. This was achieved by using the appropriate barrier parameters in the reduction procedures. We found that the enhancement due to the barrier lowering and the suppression arising from breakup couplings depend exclusively on the breakup threshold. Further, the strength of these effects grows as the threshold decreases.

However, these conclusions are based on a very limited set of systems. Further studies involving other neutron-rich projectiles and lighter targets are called for.

ACKNOWLEDGMENTS

Work supported in part by the Brazilian funding agencies, CNPq, FAPERJ, CAPES, and the INCT-FNA (Instituto Nacional de Ciência e Tecnologia- Física Nuclear e Aplicações), Research Project No. 464898/2014-5. Enlightening discussions with Dr. Valdir Guimarães on the experiment on ^{6}He + ^{209}Bi fusion are acknowledged.

[1] L. F. Canto, P. R. S. Gomes, R. Donangelo, and M. S. Hussein, Phys. Rep. **424**, 1 (2006).
[2] N. Keeley, R. Raabe, N. Alamanos, and J. L. Sida, Prog. Part. Nucl. Phys. **59**, 579 (2007).
[3] N. Keeley, N. Alamanos, K. W. Kemper, and K. Rusek, Prog. Part. Nucl. Phys. **63**, 396 (2009).
[4] L. F. Canto, P. R. S. Gomes, R. Donangelo, J. Lubian, and M. S. Hussein, Phys. Rep. **596**, 1 (2015).
[5] J. J. Kolata, V. Guimarães, and E. F. Aguilera, Eur. Phys. J. A **52**, 123 (2016).
[6] L. Canto, V. Guimarães, J. Lubian, and M. Hussein, Eur. Phys. J. A **56**, 281 (2020).
[7] K. Hagino, K. Ogata, and A. M. Moro, Prog. Part. Nucl. Phys. **125**, 103951 (2022).
[8] M. Dasgupta, D. J. Hinde, K. Hagino, S. B. Moraes, P. R. S. Gomes, R. M. Anjos, R. D. Butt, A. C. Berriman, N. Carlin, C. R. Morton *et al.*, Phys. Rev. C **66**, 041602(R) (2002).
[9] K. Hagino, M. Dasgupta, and D. J. Hinde, Nucl. Phys. A **738**, 475 (2004).
[10] A. Diaz-Torres, D. J. Hinde, J. A. Tostevin, M. Dasgupta, and L. R. Gasques, Phys. Rev. Lett. **98**, 152701 (2007).
[11] A. Diaz-Torres, J. Phys. G: Nucl. Part. Phys. **37**, 075109 (2010).
[12] A. Diaz-Torres, Comput. Phys. Commun. **182**, 1100 (2011).
[13] H. D. Marta, L. F. Canto, and R. Donangelo, Phys. Rev. C **89**, 034625 (2014).
[14] G. D. Kolinger, L. F. Canto, R. Donangelo, and S. R. Souza, Phys. Rev. C **98**, 044604 (2018).
[15] N. Keeley, K. W. Kemper, and K. Rusek, Phys. Rev. C **65**, 014601 (2001).
[16] A. Diaz-Torres, I. J. Thompson, and C. Beck, Phys. Rev. C **68**, 044607 (2003).
[17] P. Descouvemont, T. Druet, L. F. Canto, and M. S. Hussein, Phys. Rev. C **91**, 024606 (2015).
[18] K. Hagino, A. Vitturi, C. H. Dasso, and S. M. Lenzi, Phys. Rev. C **61**, 037602 (2000).
[19] A. Diaz-Torres and I. J. Thompson, Phys. Rev. C **65**, 024606 (2002).
[20] J. Rangel, M. Cortes, J. Lubian, and L. F. Canto, Phys. Lett. B **803**, 135337 (2020).
[21] M. R. Cortes, J. Rangel, J. L. Ferreira, J. Lubian, and L. F. Canto, Phys. Rev. C **102**, 064628 (2020).
[22] S. Hashimoto, K. Ogata, S. Chiba, and M. Yahiro, Prog. Theor. Phys. **122**, 1291 (2009).
[23] V. V. Parkar, V. Jha, and S. Kailas, Phys. Rev. C **94**, 024609 (2016).
[24] M. Boselli and A. Diaz-Torres, J. Phys. G: Nucl. Part. Phys. **41**, 094001 (2014).
[25] M. Boselli and A. Diaz-Torres, Phys. Rev. C **92**, 044610 (2015).
[26] J. Lei and A. M. Moro, Phys. Rev. Lett. **122**, 042503 (2019).

[27] M. Ichimura, N. Austern, and C. M. Vincent, Phys. Rev. C **32**, 431 (1985).

[28] J. Lubian, J. L. Ferreira, J. Rangel, M. R. Cortes, and L. F. Canto, Phys. Rev. C **105**, 054601 (2022).

[29] M. Dasgupta, P. R. S. Gomes, D. J. Hinde, S. B. Moraes, R. M. Anjos, A. C. Berriman, R. D. Butt, N. Carlin, J. Lubian, C. R. Morton *et al.*, Phys. Rev. C **70**, 024606 (2004).

[30] A. Mukherjee, S. Roy, M. K. Pradhan, M. S. Sarkar, P. Basu, B. Dasmahapatra, T. Bhattacharya, S. Bhatacharya, S. K. Basu, A. Chatterjee *et al.*, Phys. Lett. B **636**, 91 (2006).

[31] R. Broda, M. Ishihara, B. Herskind, H. Oeschler, S. Ogaza, and H. Ryde, Nucl. Phys. A **248**, 356 (1975).

[32] M. K. Pradhan, A. Mukherjee, P. Basu, A. Goswami, R. Kshetri, R. Palit, V. V. Parkar, M. Ray, S. Roy, P. R. Chowdhury, M. S. Sarkar, and S. Santra, Phys. Rev. C **83**, 064606 (2011).

[33] P. K. Rath, S. Santra, N. L. Singh, B. K. Nayak, K. Mahata, R. Palit, K. Ramachandran, S. K. Pandit, A. Parihari, A. Pal *et al.*, Phys. Rev. C **88**, 044617 (2013).

[34] P. K. Rath, S. Santra, N. L. Singh, R. Tripathi, V. V. Parkar, B. K. Nayak, K. Mahata, R. Palit, S. Kumar, S. Mukherjee *et al.*, Phys. Rev. C **79**, 051601(R) (2009).

[35] P. K. Rath, S. Santra, N. L. Singh, K. Mahata, R. Palit, B. K. Nayak, K. Ramachandran, V. V. Parkar, R. Tripathi, S. K. Pandit *et al.*, Nucl. Phys. A **874**, 14 (2012).

[36] I. J. Thompson, M. A. Nagarajan, J. A. Lilley, and M. J. Smithson, Nucl. Phys. A **505**, 84 (1989).

[37] A. Shrivastava, A. Navin, A. Diaz-Torres, V. Nanal, K. Ramachandran, M. Rejmund, S. Bhattacharyya, A. Chatterjee, S. Kailas, A. Lemasson *et al.*, Phys. Lett. B **718**, 931 (2013).

[38] A. Shrivastava, A. Navin, A. Lemasson, K. Ramachandran, V. Nanal, M. Rejmund, K. Hagino, T. Ichikawa, S. Bhattacharyya, A. Chatterjee, S. Kailas, K. Mahata, V. V. Parkar, R. G. Pillay, and P. C. Rout, Phys. Rev. Lett. **103**, 232702 (2009).

[39] C. L. Guo, G. L. Zhang, S. P. Hu, J. C. Yang, H. Q. Zhang, P. R. S. Gomes, J. Lubian, X. G. Wu, J. Zhong, C. Y. He *et al.*, Phys. Rev. C **92**, 014615 (2015).

[40] H. Kumawat, V. Jha, V. V. Parkar, B. J. Roy, S. K. Pandit, R. Palit, P. K. Rath, C. S. Palshetkar, S. K. Sharma, S. Thakur, A. K. Mohanty, A. Chatterjee, and S. Kailas, Phys. Rev. C **86**, 024607 (2012).

[41] V. V. Parkar, S. K. Sharma, R. Palit, S. Upadhyaya, A. Shrivastava, S. K. Pandit, K. Mahata, V. Jha, S. Santra, K. Ramachandran *et al.*, Phys. Rev. C **97**, 014607 (2018).

[42] C. S. Palshetkar, S. Thakur, V. Nanal, A. Shrivastava, N. Dokania, V. Singh, V. V. Parkar, P. C. Rout, R. Palit, R. G. Pillay, S. Bhattacharyya, A. Chatterjee, S. Santra, K. Ramachandran, and N. L. Singh, Phys. Rev. C **89**, 024607 (2014).

[43] M. Dasgupta, D. J. Hinde, R. D. Butt, R. M. Anjos, A. C. Berriman, N. Carlin, P. R. S. Gomes, C. R. Morton, J. O. Newton, A. Szanto de Toledo *et al.*, Phys. Rev. Lett. **82**, 1395 (1999).

[44] C. S. Palshetkar, S. Santra, A. Chatterjee, K. Ramachandran, S. Thakur, S. K. Pandit, K. Mahata, A. Shrivastava, V. V. Parkar, and V. Nanal, Phys. Rev. C **82**, 044608 (2010).

[45] P. R. S. Gomes, I. Padrón, E. Crema, O. A. Capurro, J. O. F. Niello, G. V. Martí, A. Arazi, M. Trotta, J. Lubian, M. E. Ortega *et al.*, Phys. Lett. B **634**, 356 (2006).

[46] P. R. S. Gomes, I. Padron, E. Crema, O. A. Capurro, J. O. Fernández Niello, A. Arazi, G. V. Marti, J. Lubian, M. Trotta, A. J. Pacheco, J. E. Testoni, M. D. Rodríguez, M. E. Ortega, L. C. Chamon, R. M. Anjos, R. Veiga, M. Dasgupta, D. J. Hinde, and K. Hagino, Phys. Rev. C **73**, 064606 (2006).

[47] Y. D. Fang, P. R. S. Gomes, J. Lubian, X. H. Zhou, Y. H. Zhang, J. L. Han, M. L. Liu, Y. Zheng, S. Guo, J. G. Wang *et al.*, Phys. Rev. C **87**, 024604 (2013).

[48] Y. D. Fang, P. R. S. Gomes, J. Lubian, M. L. Liu, X. H. Zhou, D. R. Mendes Junior, N. T. Zhang, Y. H. Zhang, G. S. Li, J. G. Wang *et al.*, Phys. Rev. C **91**, 014608 (2015).

[49] N. T. Zhang, Y. D. Fang, P. R. S. Gomes, J. Lubian, M. L. Liu, X. H. Zhou, G. S. Li, J. G. Wang, S. Guo, Y. H. Qiang *et al.*, Phys. Rev. C **90**, 024621 (2014).

[50] M. Dasgupta, D. J. Hinde, S. L. Sheehy, and B. Bouriquet, Phys. Rev. C **81**, 024608 (2010).

[51] G. S. Li, J. G. Wang, J. Lubian, H. O. Soler, Y. D. Fang, M. L. Liu, N. T. Zhang, X. H. Zhou, Y. H. Zhang, B. S. Gao *et al.*, Phys. Rev. C **100**, 054601 (2019).

[52] F. Gollan, D. Abriola, A. Arazi, M. A. Cardona, E. de Barbará, J. de Jesús, D. Hojman, R. M. Betan, J. Lubian, A. J. Pacheco, B. Paes, D. Schneider, and H. O. Soler, Phys. Rev. C **104**, 024609 (2021).

[53] M. Kaushik, G. Gupta, S. Thakur, H. Krishnamoorthy, P. P. Singh, V. V. Parkar, V. Nanal, A. Shrivastava, R. G. Pillay, K. Mahata *et al.*, Phys. Rev. C **101**, 034611 (2020).

[54] J. J. Kolata, V. Guimarães, D. Peterson, P. Santi, R. White-Stevens, J. von Schwarzenberg, J. D. Hinnefeld, E. F. Aguilera, E. Martinez-Quiroz, D. A. Roberts *et al.*, Phys. Rev. C **57**, R6(R) (1998).

[55] P. A. DeYoung, B. Hughey, P. L. Jolivette, G. F. Peaslee, J. J. Kolata, V. Guimarães, D. Peterson, P. Santi, H. C. Griffin, J. A. Zimmerman *et al.*, Phys. Rev. C **58**, 3442 (1998).

[56] L. F. Canto, P. R. S. Gomes, J. Lubian, L. C. Chamon, and E. Crema, Nucl. Phys. A **821**, 51 (2009).

[57] M. Trotta, J. L. Sida, N. Alamanos, A. Andreyev, F. Auger, D. L. Balabanski, C. Borcea, N. Coulier, A. Drouart, D. J. C. Durand, G. Georgiev, A. Gillibert, J. D. Hinnefeld, M. Huyse, C. Jouanne, V. Lapoux, A. Lepine, A. Lumbroso, F. Marie, A. Musumarra, G. Neyens, S. Ottini, R. Raabe, S. Ternier, P. Van Duppen, K. Vyvey, C. Volant, and R. Wolski, Phys. Rev. Lett. **84**, 2342 (2000).

[58] R. Raabe, J. L. Sida, J. L. Chavet, N. Alamanos, C. Angulo, J. M. Casandjian, S. Courtin, A. Drouart, C. Durand, P. Figuera *et al.*, Nature **431**, 823 (2004).

[59] C. Signorini, A. Yoshida, Y. Watanabe, D. Pierroutsakou, L. Stroe, T. Fukuda, M. Mazzocco, N. Fukuda, Y. Mizoi, M. Ishihara *et al.*, Nucl. Phys. A **735**, 329 (2004).

[60] Y. E. Penionzhkevich, R. Astabatyan, N. Demekhina, G. Gulbekian, R. Kalpakchieva, A. A. Kulko, S. Lukyanov, E. R. Markaryan, V. Maslov, Y. E. R. Muzychka *et al.*, Eur. Phys. J. A **31**, 185 (2007).

[61] M. Arnould, S. Goriely, and K. Takahashi, Phys. Rep. **450**, 97 (2007).

[62] L. F. Canto, P. R. S. Gomes, J. Lubian, L. C. Chamon, and E. Crema, J. Phys. G: Nucl. Part. Phys. **36**, 015109 (2009).

[63] Y. Sakuragi, M. Yahiro, and M. Kamimura, Prog. Theor. Phys. **70**, 1047 (1983).

[64] Y. Sakuragi, M. Yahiro, and M. Kamimura, Prog. Theor. Phys. Suppl. **89**, 136 (1986).

[65] N. Austern, Y. Iseri, M. Kamimura, M. Kawai, G. Rawitscher, and M. Yashiro, Phys. Rep. **154**, 125 (1987).

[66] I. J. Thompson, Comput. Phys. Rep. **7**, 167 (1988).

[67] L. C. Chamon, D. Pereira, M. S. Hussein, M. A. Candido Ribeiro, and D. Galetti, Phys. Rev. Lett. **79**, 5218 (1997).
[68] L. C. Chamon, B. V. Carlson, L. R. Gasques, D. Pereira, C. De Conti, M. A. G. Alvarez, M. S. Hussein, M. A. Cândido Ribeiro, E. S. Rossi, Jr., and C. P. Silva, Phys. Rev. C **66**, 014610 (2002).
[69] L. F. Canto and M. S. Hussein, *Scattering Theory of Molecules, Atoms and Nuclei* (World Scientific Publishing Co. Pte. Ltd., Singapore, 2013).
[70] L. F. Canto, D. R. Mendes Junior, P. R. S. Gomes, and J. Lubian, Phys. Rev. C **92**, 014626 (2015).
[71] C. Y. Wong, Phys. Rev. Lett. **31**, 766 (1973).
[72] A. Di Pietro, V. Scuderi, A. M. Moro, L. Acosta, F. Amorini, M. J. G. Borge, P. Figuera, M. Fisichella, L. M. Fraile, J. Gomez-Camacho *et al.*, Phys. Rev. C **85**, 054607 (2012).
[73] P. Capel, G. Goldstein, and D. Baye, Phys. Rev. C **70**, 064605 (2004).
[74] A. Yoshida, C. Signorini, T. Fukuda, Y. Watanabe, N. Aoi, M. Hirai, M. Ishihara, H. Kobinata, Y. Mozoi, L. Muller *et al.*, Phys. Lett. B **389**, 457 (1996).
[75] T. Matsumoto, E. Hiyama, K. Ogata, Y. Iseri, M. Kamimura, S. Chiba, and M. Yahiro, Phys. Rev. C **70**, 061601(R) (2004).
[76] A. M. Moro, K. Rusek, J. M. Arias, J. Gómez-Camacho, and M. Rodríguez-Gallardo, Phys. Rev. C **75**, 064607 (2007).
[77] M. Rodríguez-Gallardo, J. M. Arias, J. Gómez-Camacho, R. C. Johnson, A. M. Moro, I. J. Thompson, and J. A. Tostevin, Phys. Rev. C **77**, 064609 (2008).
[78] J. P. Fernández-García, A. Di Pietro, P. Figuera, J. Gómez-Camacho, M. Lattuada, J. Lei, A. M. Moro, M. Rodríguez-Gallardo, and V. Scuderi, Phys. Rev. C **99**, 054605 (2019).